Three-Dimensional Structure in Lipid Micelles of the Pediocin-like Antimicrobial Peptide Sakacin P and a Sakacin P Variant That Is Structurally Stabilized by an Inserted C-Terminal Disulfide Bridge†

Marianne Uteng,§ Håvard H. Hauge,§ Phineus R. L. Markwick,|| Gunnar Fimland,§ Dimitris Mantzilas,§ Jon Nissen-Meyer,§ and Claudia Muhle-Goll*,||,$

Department of Biochemistry, University of Oslo, Oslo, Norway, European Molecular Biology Laboratory, Meyerhofstrasse 1, D-69117 Heidelberg, Germany, and Institut für Anästhesiologie & Operative Intensivmedizin, Universitätsklinikum Mannheim, Theodor-Kutzer-Ufer, D-68135 Mannheim, Germany

Received April 10, 2003; Revised Manuscript Received July 23, 2003

ABSTRACT: The three-dimensional structures in dodecylphosphocholine (DPC) micelles and in trifluoroethanol (TFE) of the pediocin-like antimicrobial peptide sakacin P and an engineered variant of sakacin P (termed sakP[N24C+44C]) have been determined by use of nuclear magnetic resonance spectroscopy. SakP[N24C+44C] has an inserted non-native activity- and structure-stabilizing C-terminal disulfide bridge that ties the C-terminus to the middle part of the peptide. In the presence of DPC, the cationic N-terminal region (residues 1−17) of both peptides has an S-shaped conformation that is reminiscent of a three-stranded antiparallel β-sheet and that is more pronounced when the peptide was dissolved in TFE instead of DPC. The four positively charged residues located in the N-terminal part are found pointing to the same direction. For both peptides, the N-terminal region is followed by a well-defined central amphiphilic α-helix (residues 18−33), and this in turn is followed by the C-terminal tail (residues 34−43 for sakacin P and 34−44 for sakP[N24C+44C]) that lacks any apparent common secondary structural motif. In the presence of DPC, the C-terminal tails in both peptides fold back onto the central α-helix, thereby creating a hairpin-like structure in the C-terminal halves. The lack of long-range NOEs between the β-sheet N-terminal region and the hairpin-like C-terminal half indicates that there is a flexible hinge between these regions. We discuss which implications such a structural arrangement has on the interaction with the target cell membrane.

Many Gram-positive bacteria produce antimicrobial peptides (AMPs),[1] generally termed bacteriocins. These peptides are usually cationic, less than 50 amino acid residues long, and contain an amphiphilic or hydrophobic region (*1*−*3*). AMPs with these characteristics are also produced by plants and a wide variety of animals, including humans, and are thus widely distributed in nature (*1*). One important group of AMPs consists of the pediocin-like peptides (class IIa bacteriocins) produced by lactic acid bacteria (*3*−*5*). Today, at least 20 members of this group are characterized (*3*−*6*). The pediocin-like AMPs contain between 37 and 48 residues, and they are cationic, display anti-listeria activity, and kill target cells by permeabilizing the cell membrane (*7*, *8*). In their N-terminal region, they all have a disulfide bridge (most often from residue 9 to 14) and an YGNGV/L sequence-motif. Despite their high sequence similarity (between 40 and 90%), they differ markedly with respect to the bacteria they kill (i.e. their target cell specificity) (*3*, *9*−*13*). It appears that the mostly amphiphilic C-terminal half of these peptides is especially important in determining the target cell specificity, since hybrid bacteriocins containing N- and C-terminal regions from different pediocin-like peptides have a target cell specificity similar to that of the peptide from which the C-terminal region is derived (*10*).

The three-dimensional structures of two pediocin-like AMPs, the 37-mer leucocin A and the 48-mer carnobacteriocin B2, have been analyzed by NMR spectroscopy (*14*, *15*). Under membrane-mimicking conditions, the N-terminal region of leucocin A had a well-structured three-stranded antiparallel β-sheet conformation (stabilized by the 9 to 14 disulfide bridge), whereas this region in carnobacteriocin B2 was disordered. Both peptides contained a central amphiphilic α-helix, whereas the C-terminal tail was found to be rather unstructured for both peptides (*14*, *15*).

Information on the role and position of the apparently unstructured C-terminal tail that varies considerably in the different subgroups may be deduced from studies dealing with the second disulfide bridge that is present in the

† This work was supported by a grant from the Norwegian Research Council.

* To whom correspondence should be addressed. Telephone: +49-6221-387397. Fax: +49-6221-387306. E-mail: muhle@embl-heidelberg.de.

§ University of Oslo.

|| European Molecular Biology Laboratory.

$ Universitätsklinikum Mannheim.

[1] Abbreviations: AMP, antimicrobial peptide; CD, circular dichroism; DPC, dodecylphosphocholine; LAB, lactic acid bacteria; MALDI TOF, matrix assisted laser desorbtion time-of-flight; NMR, nuclear magnetic resonance; NOE, nuclear Overhauser effect; NOESY, two-dimensional nuclear Overhauser correlation spectroscopy; rmsd, root-mean-square deviation; TFA, trifluoroacetic acid; TFE, trifluoroethanol; TOCSY, total correlation spectroscopy.

10.1021/bi034572i CCC: $25.00
Published on Web 09/13/2003

C-terminal region in a few pediocin-like AMPs, such as pediocin PA-1. This C-terminal disulfide bridge connects the C-terminal end with the central α-helical region. Fimland et al. showed that the introduction of the C-terminal disulfide bridge into sakacin P particularly broadened the target cell specificity and increased the potency at elevated temperatures, while removing the C-terminal disulfide bridge in pediocin PA-1 by Cys to Ser mutations decreased its potency and stability (*12*). This raised the question whether the pediocin-like AMPs in fact adopt in their C-terminal region a more structured and compact conformation than has previously been detected by NMR analysis. To obtain more insight into the structure of pediocin-like AMPs, in this study we have analyzed by NMR spectroscopy the three-dimensional structure of both sakacin P and a sakacin P variant, termed sakP[N24C+44C], in which an activity- and structure-stabilizing C-terminal disulfide bridge has been inserted.

MATERIALS AND METHODS

Bacterial Strains and Culture Conditions. Lactobacillus sake NCDO 2714 was used as indicator strain in the activity assays and was cultured in MRS broth (Oxoid) at 30 °C. *L. sake* Lb790/pMLS114 (*16)* was used for production of sakacin P, and *L. sake* Lb790/pGF10 was used for production of sakP[N24C+44C]. pGF10 is a pMG36e derived plasmid (*17*) containing the sakP[N24C+44C] gene (*sppA*) and sakacin P immunity gene (*spiA*) (*16*) fused to the genes encoding the secretion apparatus of pediocin PA-1 (*papC and papD*) (*4*). Cultures producing bacteriocins were started by inoculating 2 L of MRS broth (supplemented with yeast extract (Merck) and glucose to final concentrations of 6 and 10 g/L, respectively) with cells that had been stored at −80 °C. The inoculated medium was first incubated at 30 °C for 12 h to initiate cell growth and then transferred to room temperature (about 22 °C) and incubated for 24 h, after which the cultures had reached stationary phase and were ready for AMP purification.

Purification of AMPs and AMP Assay. Sakacin P and sakP[N24C+44C] were each purified to homogeneity from approximately 10 L of culture by applying the bacteria culture directly on a cation exchanger followed by reverse-phase chromatography, as described previously (*18*). The primary structures and purity of the peptides were confirmed by mass spectrometry using a MALDI-TOF Voyager-DERP mass spectrometer (Perseptive Biosystems) with α-cyano-4-hydroxycinnamic acid as matrix, by analytical reverse-phase chromatography using a μRPC SC 2.1/10 C_2/C_{18} column (Amersham Biosciences) on the SMART chromatography system (Amersham Biosciences), and by capillary electrophoresis using an untreated silica capillary (75 μM × 20 cm; Beckman P/ACE system 2050). Peptide concentrations were calculated from the absorbance at 280 nm using the molar extinction coefficients (*6*).

AMP activity was determined using a microtiter plate assay system, essentially as described earlier (*6*).

CD Spectroscopy. CD spectra were recorded using a Jasco J-810 spectrometer calibrated with ammonium D-camphor-10-sulfonate. Both peptides were solubilized in water with 0.1% (v/v) TFA. The measurements were performed at temperatures from 12 to 52 °C in the presence of TFE (0−90% v/v) or DPC (2−14 mM) with a peptide concentration of 0.1 mg/mL. A quartz cuvette with a path length of 1 mm was used. Samples were scanned three to six times at 20 nm/min with a time constant of 2 s and a slit width of 2 nm, over the wavelength range 190−260 nm. The data were averaged, and the spectrum of a protein-free control sample was subtracted, thus giving the mean residual ellipticity of the peptide.

The α-helical contents of the peptides at various temperatures and solvent conditions were calculated from the mean residual ellipticity at 222 nm ($[\theta]_{222}$) by using the formula

$$\times c4_H = [\theta]_{222}/[-39500(1 - 2.57/n)]$$

where $\times c4_H$ represents the α-helical content and n represents the number of peptide bonds (*19*). All measurements were conducted at least twice, and crucial measurements were repeated several times, until the standard deviations in the percentage of helicity were below 2%.

NMR Sample Preparation. For analyses in DPC, the peptides were dissolved in 700 μL of 250 mM deuterated DPC (CDN Isotopes) and 10% deuterated water (Cambridge Isotope Laboratories) to a final concentration of 1 mM. The sample was acidified by adding TFA to a final concentration of 0.1%, thus obtaining a pH of about 2.8. For analysis in TFE, sakacin P was dissolved in 90% TFE, 0.1% TFA, and 10% deuterated water to a final concentration of 1 mM.

NMR Spectroscopy. NMR spectra of sakacin P and sakP-[N24C+44C] in DPC were acquired at 25 °C on either a Bruker DRX500 or DRX600 spectrometer equipped with a cryoprobe. Supplementary information was obtained by recording spectra at 35 and 45 °C to resolve spectral overlap. TOCSY spectra were measured using the DIPSI-2rc sequence (*20*). Water suppression was achieved by applying the WATERGATE pulse sequence (*21*). A series of mixing times between 40 and 65 ms was used for the TOCSY spectra; NOESY spectra were acquired with a 150 ms mixing time for structure calculation and a 200 ms mixing time to facilitate sequential assignment. In the case of sakacin P, additional NOESY and TOCSY spectra were obtained in 90% TFE at 25 °C with mixing times of 150 and 200 ms (NOESY) and 64 ms (TOCSY), respectively.

Spectral data were recorded with 512 to 800 increments in the t1 dimensions, 2048 complex data points in t2, and 16−32 scans. Prior to Fourier transformation, the data matrix was zero-filled to 2K × 1K complex points and multiplied by a Gaussian (F2) or sine bell (F1) window function. Data were processed using the Bruker XWIN-NMR software (version 2.6) and analyzed with XEASY (*22*). Integration of NOE correlations observed in NOESY spectra with a 150 ms mixing time was obtained in XEASY using the "maximum integration" mode of XEASY. Hydrogen bond restraints (range 1.8−2.8 Å) were included in the structure calculations at a later stage. These restraints were determined on the basis of structural NOE patterns in the α-helical region and comprised the range of residues 18−33.

Restraints and Structure Calculation. Structure calculation was performed with a simulated annealing protocol using CNS (version 1.1) (*23*) and the standard protocol of ARIA (version 1.2) (*24*). The "parallhdg.pro" force field (version 5.3) was used to describe the covalent and nonbonded interactions for the polypeptide (*25*). The structures were calculated using a simulated annealing profile comprising

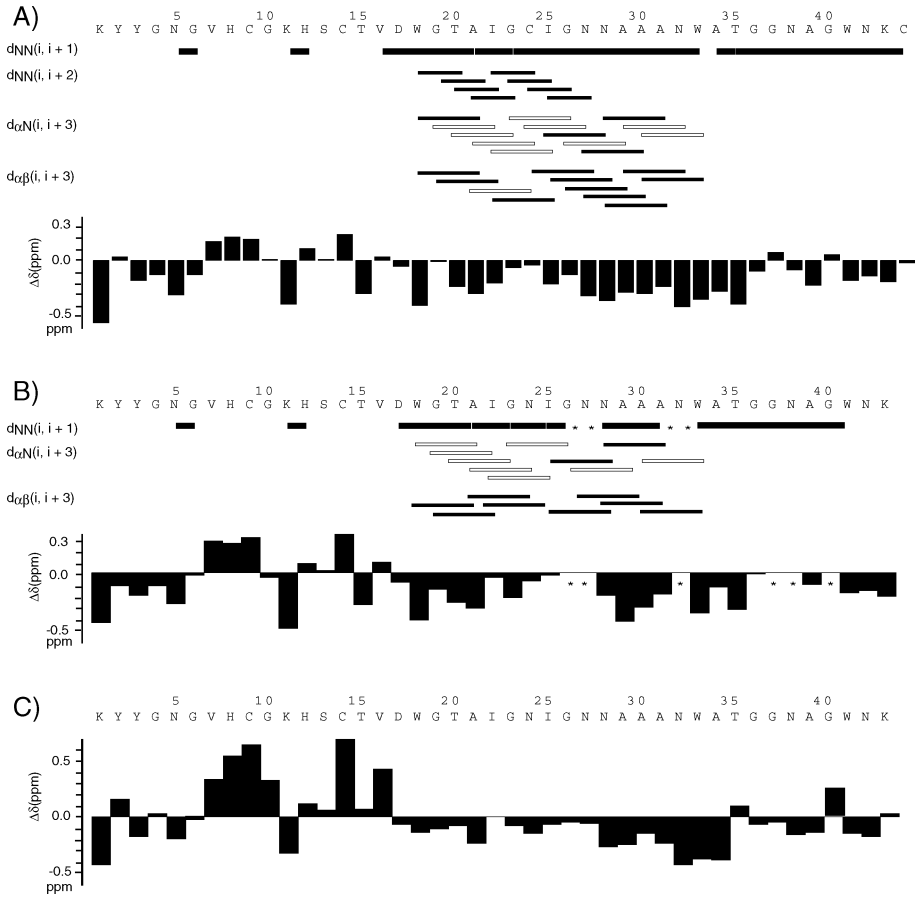

FIGURE 1: Pattern of interresidue NOEs observed at a 150 ms mixing time for (A) sakP[N24C+44C] and (B) sakacin P in DPC micelles. Open boxes show areas where spectral overlap prevented unambiguous assignment. Below, the deviation of the H_α chemical shifts from random coil values is shown for each peptide. Asterisks (*) mark those residues whose H_N frequency could not be determined due to spectral overlap. Due to spectral overlap, NOEs of the type $H_N-H_N(i, i+2)$ could not be determined for sakacin P. (C) Sakacin P in 90% TFE. Since the pattern of interresidue NOEs is comparable to that of sakP[N24C+44C], only the deviation of the H_α chemical shifts from random coil values is shown.

four stages: a high temperature conformational search phase in torsion angle dynamics (50 ps at 10 000 K with a 45 fs time step), two cooling phases (10 000 to 2000 K in 25 ps with torsion angle dynamics, and 1000 to 50 K in 20 ps with Cartesian dynamics, each with a 5 fs time step), and a final minimization phase. Floating chirality assignment of prochiral groups was applied as described (*25*). A total of 50 structures were generated in the final calculation, of which the 20 best structures were further refined in water. We used a total of 599 distance restraints (280 intraresidual, 184 sequential, 91 medium range, and 44 long range) for sakP[N24C+44C], 349 distance restraints (194 intraresidual, 90 sequential, 43 medium range, and 22 long range) for sakacin P in DPC micelles, and 522 distance restraints (292 intraresidual, 109 sequential, 82 medium range, and 39 long range) for sakacin P in 90% TFE plus additionally 13 bond restraints, that were derived from the pattern of interresidue NOEs shown in Figure 1 for the final calculation of conformers.

Restrained simulated annealing was performed on the 10 lowest energy structures of each sakP[N24C+44C] in DPC, sakacin P in DPC, and in 90% TFE using the SANDER module of the AMBER 6 package (*26*). Both ambiguous and unambiguous NOE-derived distance restraints were employed with an energy constant of 32 kcal mol^{-1} $Å^{-1}$ using the standard AMBER flat bottom NOE potential defined with the parabolic region extending to 0.5 Å below/above the lower/upper distance bounds. The simulated annealing protocol consisted of rapid heating to 1200 K in the first 200 ps. This was followed by slow cooling to 200 K for 800 ps and rapid cooling to 0 K for 200 ps. A generalized Born solvation model was used with a modified set of Bondi radii and screening parameters adopted from the Tinker programs (*27*). A nonbonded electrostatic cutoff of 20 Å was employed.

The structures were superimposed onto the secondary structure backbone heavy atoms of the lowest energy structure. The structural models were visualized with the program MOLMOL (*28*).

RESULTS

CD Measurements. The sequences of sakacin P and the sakacin P variant, sakP[N24C+44C], in which an activity- and structure-stabilizing disulfide bridge has been inserted by adding a cysteine residue at position 44 and replacing Asn24 in sakacin P with a cysteine residue can be derived from Figure 1. To find optimal conditions for recording NMR spectra, the two peptides were first analyzed by CD spectroscopy at various temperatures in various membrane-mimicking environments. The analysis revealed that both peptides are unstructured in water but tend to become structured in the presence of TFE and membrane-mimicking agents such as DPC. There was a gradual increase in helicity upon increasing the TFE concentration to 50% in the case

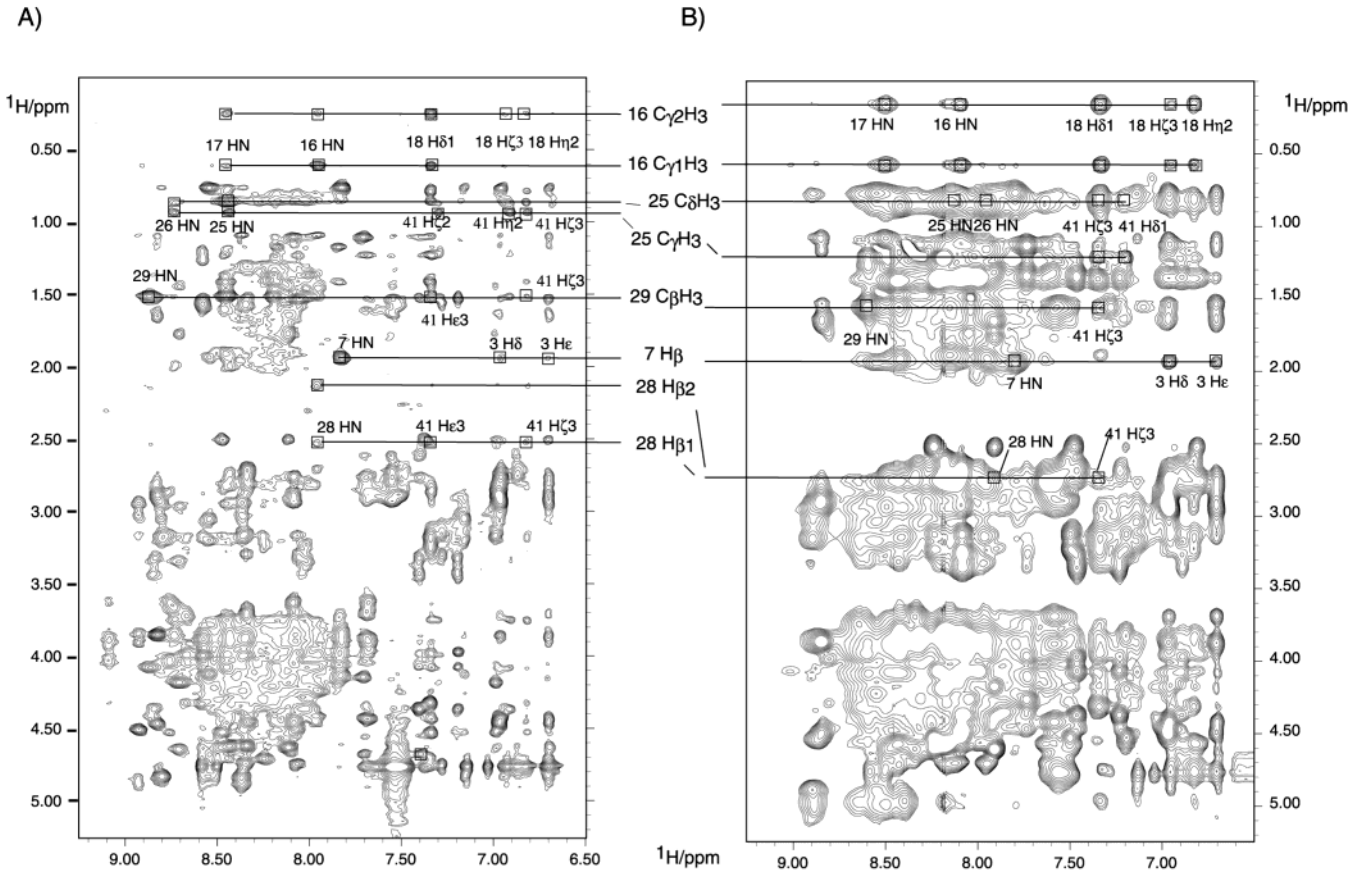

FIGURE 2: NOESY fingerprint region of the spectra of (A) sakP[N24C+44C] and (B) sakacin P in 250 mM DPC micelles at 25 °C. The mixing time was 150 ms each. NOE cross-peaks that indicate that the C-terminal tail folds back are boxed. The assignment in ω1 is marked with a straight line for the two spectra; the corresponding assignment in ω2 is found next to the peaks.

of sakacin P and to 75% in the case of sakP[N24C+44C]. No further significant alterations in the helicity were observed upon increasing the TFE concentration to 90%. Interestingly, sakP[N24C+44C] had a higher α-helical content than sakacin P at all TFE concentrations tested (38% helicity as compared to 33% in 50% TFE, and 48% helicity as compared to 33% in 75% TFE; all at 22 °C). DPC at concentrations above the critical micelle concentration (1 mM) also induced α-helical structuring in both peptides. Again a higher degree of helicity was observed for sakP[N24C+44C] than sakacin P (29% helicity as compared to 14% in 2 mM DPC, and 34% helicity as compared to 22% and 24% in 8 and 14 mM DPC, respectively; all at 22 °C). DPC was preferentially used for structure determination by NMR, since it forms micelles and is thus a better membrane-mimicking agent than TFE. NMR spectra of sakacin P in 90% TFE/10% D_2O were, however, also recorded to account for the observed differences in the α-helical content. It also turned out that TFE was more optimal for structuring the β-sheetlike structure found in the N-terminal half of sakacin P and sakP-[N24C+44C].

Since several NMR spectra had to be taken at elevated temperatures (35, 45, and 55 °C) in order to solve ambiguities due to overlapping peaks, CD analysis was also used to investigate to what extent the peptides preserved their structuring upon increasing the temperature. When going from 12 to 52 °C in the presence of 5.5 mM DPC (which corresponds to the amount of DPC relative to the amount of peptide used in the NMR experiments), the helical content was gradually reduced from 26 to 12% for sakacin P and from 37 to 21% for sakP[N24C+44C]. The same temperature shift in the presence of 90% TFE (concentration used in the NMR experiments) gradually reduced the helical content from 33 to 23% for sakacin P and from 51 to 38% for sakP-[N24C+44C]. Thus, some structuring was retained even at 52 °C, especially in sakP[N24C+44C].

SakP[N24C+44C] in DPC: Assignment of the Proton Resonances. Using the standard procedure for sequential assignments based on homonuclear TOCSY and NOESY spectra, essentially all of the residues in the N- and C-terminal parts of sakP[N24C+44C] could be assigned. Resonance assignments for the α-helical part, however, posed problems due to the fact that the H_α and H_N resonances were close to each other. In cases of overlapping resonances, comparison of spectra recorded at different temperatures resolved most ambiguities. The spectra of sakP[N24C+44C] did not change much up to 52 °C (data not shown), although NOE cross-peaks arising from aromatic side chains gradually disappeared, reflecting the increased flexibility of the peptide chain. Line broadening for some of the amide proton resonances, especially pronounced for the amide proton of Ile22, was observed, possibly due to chemical exchange between more than one conformation (structured peptides bound to micelles and unstructured ones detached from micelles).

Figure 2A shows the NOESY fingerprint region of sakP-[N24C+44C]. An upfield shift is observed for the methyl groups of Val16 that resonate at 0.6 and 0.2 ppm (see Supporting Information) and for one of the Asn28 H_β resonances. Multiple sequence alignment has shown that the

Table 1: Structural Statistics for the Final 20 Structures of sakP[N24C+44C] and Sakacin P in DPC Micelles and Sakacin P in 90% TFE

	sakP[N24C+44C] in DPC micelles	sakacin P in DPC micelles	sakacin P in 90% TFE
	Number of NOEs		
intraresidual	280	194	292
long range	44	22	39
medium	91	43	82
sequential	280	194	109
H-bonds	13	13	13
	Root-Mean-Square Distances from Ideal Values		
bonds (Å)	4.90×10^{-3} ($\pm 0.44 \times 10^{-3}$)	3.82×10^{-3} ($\pm 0.96 \times 10^{-3}$)	4.27×10^{-3} ($\pm 0.29 \times 10^{-3}$)
angles (deg)	0.66 (±0.07)	0.54 (±0.05)	0.61 (±0.05)
impropers (deg)	2.04 (±0.28)	1.45 (±0.21)	1.81 (±0.17)
van der Waals (kcal/mol)	77.11 (±20.01)	44.71 (±10.80)	52.42 (±14.78)
	Distance Restraints		
all distance restraints	4.46×10^{-2} ($\pm 1.89 \times 10^{-2}$)	2.80×10^{-2} ($\pm 0.31 \times 10^{-2}$)	5.48×10^{-2} ($\pm 4.73 \times 10^{-2}$)
hydrogen bonds	2.63×10^{-2} ($\pm 0.80 \times 10^{-2}$)	2.15×10^{-2} ($\pm 0.94 \times 10^{-2}$)	5.27×10^{-2} ($\pm 2.11 \times 10^{-2}$)
	Nonbonded Energies		
electronic (kcal/mol)	−1452.5 (±51.4)	−1432.1 (±51.1)	−1461.3 (±48.9)
van der Waals (kcal/mol)	−237.3 (±51.4)	−264. 1 (±37.4)	−274.8 (±21.8)
	Ramachandran Deviation[a,b] (%)		
most favored	57.6	62.5	62.5
additionally allowed	33.3	28.1	25.0
generously allowed	0.0	0.2	0.0
disallowed	9.1	3.1	12.5

Global Root-Mean-Square Distance[a,c] (Å)

	sakP[N24C+44C] in DPC micelles		sakacin P in DPC micelles		sakacin P in 90% TFE	
	all atoms	backbone (N,C_α,C′)	all atoms	backbone (N,C_α,C′)	all atoms	backbone (N,C_α,C′)
1−43	4.13	3.13	4.58	3.74	5.40	4.47
18−33	1.17	0.34	1.32	0.39	1.22	0.45
6−16	2.67	1.45	2.81	1.73	2.81	1.31
1−17	3.41	1.95	3.41	2.51	3.00	1.84

[a] Ramachandran and global root-mean-square deviations were determined for the set of 10 structures that were refined in AMBER. [b] Determined by PROCHECK. [c] Calculated using MOLMOL.

tryptophans at positions 18, 33, and 41 belong to the conserved residues (*6*). Trp41, in particular, specifies a subgroup of pediocin-like AMPs that is distinct from those closely related to pediocin PA-1 who contain an additional disulfide bridge in their C-terminal half (*6*). A comparison of the chemical shifts of the three tryptophans of sakP-[N24C+44C] shows that the resonances of the aromatic ring protons of Trp18 and Trp41 are almost identical. The protons of the ring system of Trp33 are clearly distinguishable from those of Trp18 and 41 even though the differences are not high.

SakP[N24C+44C] in DPC: Identification of Secondary Structure Elements. The N-terminal part of sakP[N24C+44C] showed some medium- and long-range NOEs that indicated the presence of a three-stranded antiparallel β-sheet, extending from (and including) Lys1 to (and including) Val16. These NOEs include Lys1 H_β to Cys9 H_N, Tyr3 H_N to His8 H_α, Val7 H_α to Asn17 H_N, His8 H_N to Val16 H_α, Cys9 H_β to Cys14 H_β, Thr10 H_N to Cys14 H_α, Thr10 H_α to Ser12 H_N, and Val7 H_γ to Val16 $C_\gamma H_3$. Some of these NOEs were, however, found in overlapping regions and could therefore not be unambiguously assigned. Turns were found to be between Gly4 and Val7 and between Thr10 and Ser13, the latter turn being stabilized by the disulfide bridge between Cys9 and Cys14.

The central region of sakP[N24C+44C], from (and including) Trp18 to (and including) Trp33, is α-helical according to the $H_\alpha-H_N(i, i+3)$, $H_\alpha-H_\beta(i, i+3)$, and H_N-H_N connectivities. A pattern of interresidue NOEs for sakP-[N24C+44C] is shown in Figure 1A. Typical upfield deviations from random coil values are found for the H_α chemical shifts of residues 18 to 35 and confirm the extension of the α-helix.

Although sequential connectivities of the form $d_{NN}(i, i+1)$ were found from residue 34 to residue 44, characteristic NOEs indicative of α-helical structure, like $d_{\alpha N}(i, i+3)$, $d_{\alpha N}(i, i+4)$, and $d_{\alpha\beta}(i, i+3)$, were not observed for this region of the peptide. A few long-range NOEs were observed for the C-terminal half, confirming that the tail is tied up to the α-helix via the disulfide bridge between Cys24 and Cys44. These connections include NOEs from Ile25 $C_\gamma H_3$ and $C_\delta H_3$, Ala29 $C_\beta H_3$ and Asn28 H_β to resonances of the ring of Trp 41, respectively, as indicated in Figure 2A. The turn at the C-terminal end of the α-helix appeared to be between Trp33 and Gly36, as indicated for instance by the NOE between Asn32 H_α and Gly37 H_N.

SakP[N24C+44C] in DPC: Structure Description. We calculated 50 structures for sakP[N24C+44C], of which the 20 best structures were chosen (Table 1 and Figure 3A−C). To test the influence of the hydrogen bond restraints on the quality of the structures, the 10 best structures were subjected to an additional molecular dynamics calculation in the AMBER force field which contains an explicit electrostatic component of the force field (*26*). This showed that the omission of the hydrogen bond restraints did not change the structure. A structural ensemble of the 10 best structures calculated in AMBER is shown in Figure 3 superimposed over the backbone atoms of (A) all residues, (B) the helical

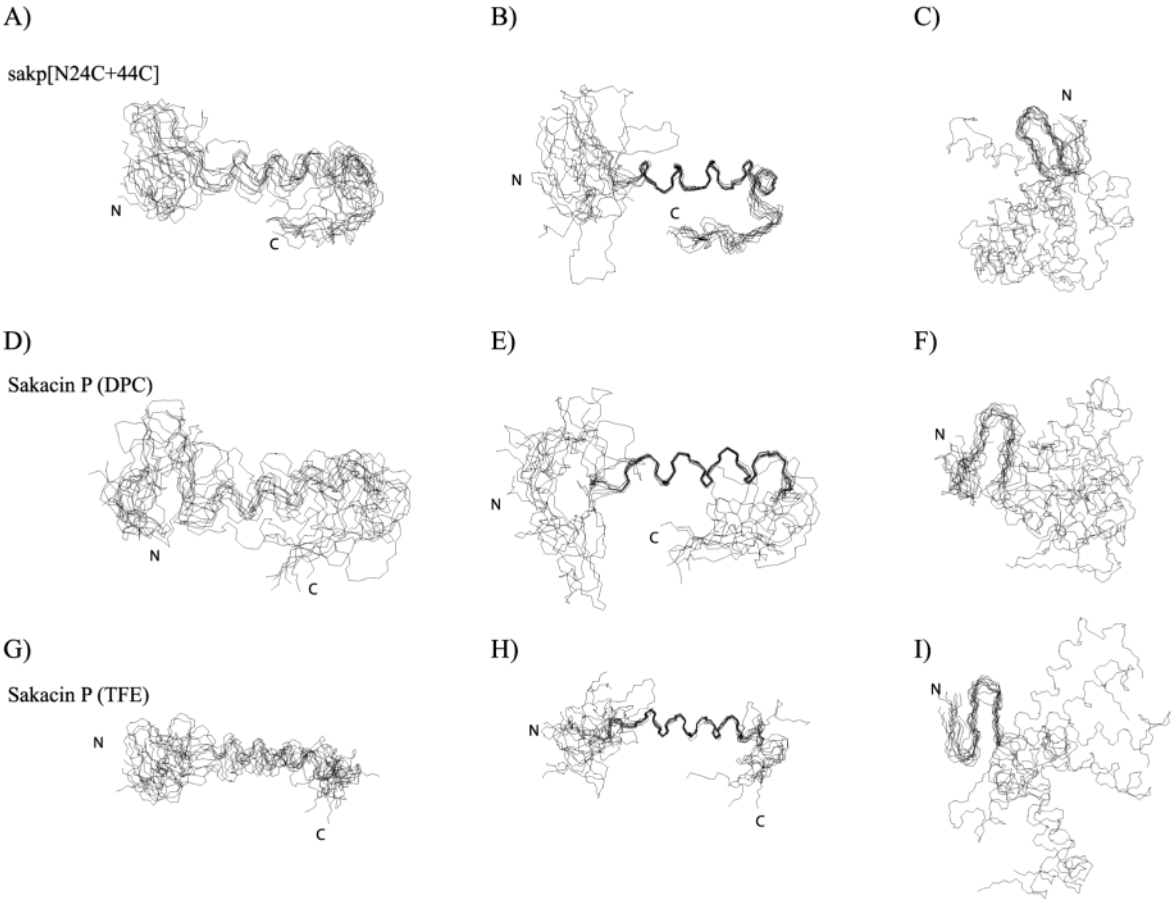

FIGURE 3: Backbone superposition of 10 structures. The structures were superposed over the backbone atoms of (A) residues 1−44, (B) residues 18−33, and (C) residues 6−16 for sakP[N24C+44C] in DPC micelles. Comparable superpositions for sakacin P in DPC micelles are shown in D−F, and those for sakacin P in 90% TFE are shown in G−I. The N- and C-termini are marked.

part (residues 18−33), and (C) the N-terminal part (6−16). The structure of sakP[N24C+44C] can be divided into three parts, the N-terminal part extending from residues 1 to 17, the central α-helix (residues 18−33), and the C-terminal part from residues 34 to 44.

In the presence of DPC, the cationic N-terminal region (residues 1−17) of sakP[N24C+44C] has an S-shaped appearance that is reminiscent of a three-stranded antiparallel *β*-sheet, although the large rmsd (1.95 Å over the backbone atoms, see Table 1) for this region indicates that the structure is relatively poorly defined. Interestingly, the positively charged residues (Lys1, His8, Lys11, and His12) in the N-terminal region are in close contact (Figure 4) and these residues, especially Lys11 and His 12, are of importance for the binding of the peptide to target cells (*11*).

The central α-helix is well defined with an rmsd of 0.34 Å over the backbone atoms (Table 1), a fact that reflects the high number of NOEs obtained for this part. The residues along the helix are arranged in an amphiphilic pattern, with Trp18, Ala21, Ile22, Ile25, Ala29, and Trp33 lying along one hydrophobic side, which is extended by Val16 and Val7 into the N-terminal part (Figure 5A). The other two ridges of the helix are formed by glycine and alanine residues (19, 23, 26, 30) along one side and polar residues (20, 24, 27, 28, and 32) along the third (Figure 5A). Together with this helix, the C-terminal tail (residues 34 to the C-terminus) forms a hairpin-like structure, since the tail folds back onto the helix, with Trp41 being buried in the interface to the

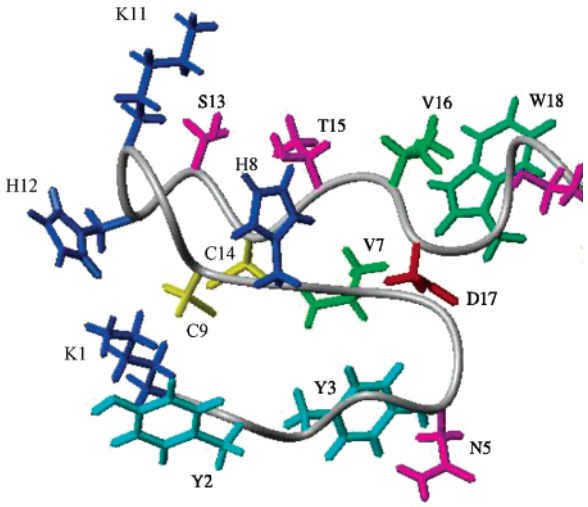

FIGURE 4: Details of the N-terminal part. The positively charged side chains of Lys1, Lys11, His12, and His8 are in close vicinity. Val16 and Trp18 interact via their hydrophobic side chains and restrict the motion between the N-terminal and the C-terminal part. Side chains are colored in green for hydrophobic (Trp, Ile, Ala, Val), magenta for polar (Asn, Thr, Ser), red for acidic (Glu), and blue for basic (Lys, His) residues. Cysteines are colored in yellow, and tyrosines, in cyan.

helix. It is in hydrophobic contact with Ile25 and partially conceals it, as well as the neighboring Ala29 and the side chain of Asn28, from the solvent. The H_β protons of Asn28 are located above the ring of Trp41 and upfield shifted. This

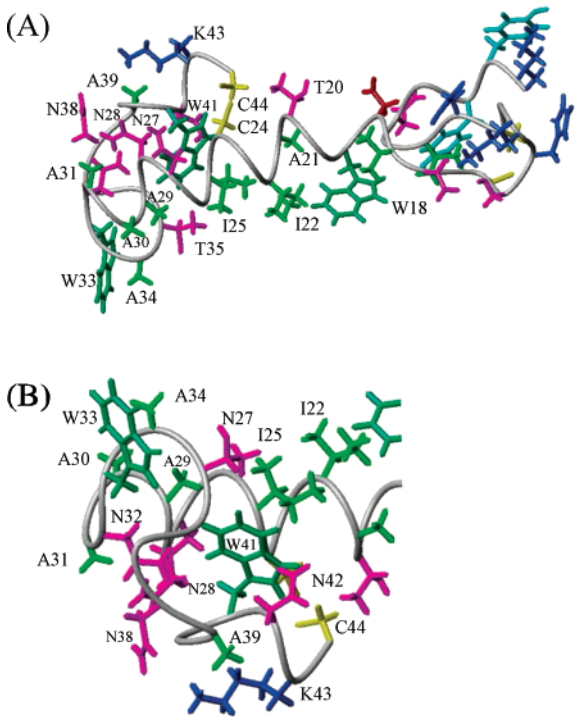

FIGURE 5: Details of the C-terminal part of sakP[N24C+44C]. (A) The side chains of residues 18−33 are arranged in an amphiphilic pattern along the α-helix of sakP[N24C+44C]. (B) Details of the hydrophobic pocket of Trp41. (Side chain coloring as in Figure 4).

interaction masks the second half of the amphiphilic helix (Figure 5B) and renders it somewhat bulky. The lack of long-range NOEs between the *β*-sheetlike structure of the N-terminal region and the hairpin-like structure formed by the central α-helix and the C-terminal tail suggests that there is a hinge at the highly conserved Asp17 residue. Motion between the two parts of the molecule is, however, partially restricted by the interaction of Val16 with Trp18, whose methyl groups are located above the ring of Trp18, as demonstrated by their upfield shift.

Sakacin P in DPC and TFE: Assignment of the Proton Resonances and Structure Description. The NOESY and TOCSY spectra of sakacin P in DPC had lower resolution (due to increased line widths) than the corresponding spectra of sakP[N24C+44C] (Figure 2B). The assignment of the proton resonances for sakacin P in DPC was thus only possible when the resonances of sakP[N24C+44C] were known. The proton chemical shifts of sakacin P were, consequently, to a large extent assigned by comparing the spectra of sakacin P with the spectra of sakP[N24C+44C]. This strategy allowed us to identify the H_N and H_α resonances and many of the side chain frequencies, although some assignments still remained unclear. The strategy was especially used to identify several of the structure-determining long-range NOEs involving connections between the side chains, the resonance frequencies of which were not otherwise sufficiently resolved to allow unambiguous assignments. For instance, the connection between Ile25 and Trp41 was identified in this manner (Figure 2B) and used to determine the approximate orientation of the C-terminal tail. The characteristic NOE pattern together with the H_α secondary shifts confirms an α-helical conformation for residues 18 to 33 (Figures 1B). On the basis of 349 distance restraints as well as 13 hydrogen bonds from residue 18 to 33, we calculated the structure of sakacin P. Figure 3D and E shows that the overall structure of the wild type resembles that of sakP[N24C+44C]. The C-terminus adopts a similar orientation as that in sakP[N24C+44C], maintained by the interaction between Trp41 and Ile25, even though with higher conformational variability (Figure 3E and Table 1). The upfield shift of one of the H_β protons of Asn28 is no longer visible (Figure 2B), indicating again the weakened interaction.

Spectra with higher resolution were obtained in 90% TFE (CD analysis showed that structuring was high at this concentration) than in DPC, and resonance assignments in TFE were consequently straightforward. The overall appearance of the spectra in DPC and TFE was similar (data not shown), although several of the H_N resonances varied in their relative positions. This most probably reflects some differences in the hydrogen bond pattern at the end of the α-helix or the level of the *β*-sheet, but it may also be due to a different arrangement of the aromatic rings or exchange phenomena. In spectra recorded in the presence of TFE, the chemical shifts of the protons in the aromatic rings in the three tryptophan residues were hardly distinguishable from each other. The H_α resonances of His8, Cys9, and Cys14 were downfield shifted compared to the DPC spectra (Figure 1C and also Supporting Information). This, together with the presence of NOE cross-peaks between the Val7 H_α and Val16 H_α, Cys9 H_α and Cys14 H_α, Val16 H_α and His8 H_N, and His8 H_α and Tyr3 H_N, indicates that the N-terminal part might fluctuate around a three-stranded antiparallel *β*-sheet conformation, although it is not well defined in terms of ϕ and ψ angles. The structures of sakacin P in TFE are shown in Figure 3 (G−I). Interestingly, the C-terminal part bends in the same direction as that in the structures determined in DPC micelles, but without a connection between Trp41 and Ile25 it loses a coherent conformation after the first turn (Figure 3H).

DISCUSSION

Despite the fact that pediocin-like AMPs share between 40 and 90% sequence homology, they each display a distinct antimicrobial spectrum of activity (*3*, *9*−*11*). How minor sequence changes result in such a variety of target cell specificity still remains an unsolved question. Possibly, these AMPs adopt a common three-dimensional fold where subtle changes in amino acid composition result in a distinct surface charge distribution and different intramolecular stabilizing interactions determine the strength of the interaction with the membrane. Among the family of AMPs, pediocin PA-1, enterocin A, coagulin, and divercin V41 are unique in the sense that they possess an extra disulfide bond involving a second pair of cysteine residues located in the C-terminal region (a multiple sequence alignment can be retrieved from ref *6*). At least for pediocin PA-1 it is known not only that it is active at higher temperatures than those for sakacin P but also that it has a broader antimicrobial spectrum (*9*) A mutant of sakacin P that contained an engineered extra C-terminal disulfide bridge comparable to pediocin PA-1 was recently shown to be likewise more tolerant against temperature and have a broader antimicrobial spectrum (*12*). The structural comparison of the wild type versus the mutant allows us to understand the subtle changes that occur upon exchange of single residues.

Comparison of the spectra of sakacin P and those of sakP-[N24C+44C] revealed that no major structural rearrangements occur by the introduction of the second disulfide bridge. Thus, it seems that the disulfide bridge introduced in sakP[N24C+44C] imposes the correct conformation on the C-terminal tail, consistent with the observation that sakP-[N24C+44C] is even more potent than sakacin P at elevated temperatures (*12*).

The observed differences in line widths for the wild type and the mutant spectra (Figure 2A and B) cannot be explained only by the large size of the DPC micelles that renders conventional 2D homonuclear magnetic resonance spectroscopy more difficult but must rely on an additional effect that adds differently to the intrinsic line broadening for each peptide. An exchange process between two different conformations that occurs with a different ratio for sakacin P and sakP[N24C+44C] would be an explanation. If we assume that the peptides exchange between a structured form bound to DPC micelles and a random conformation when detached from micelles, we can explain the different line broadening in the spectra of sakacin P and sakP[N24C+44C] by a more stable attachment to the micelles in the case of sakP[N24C+44C]. With this assumption, the different amounts of helicity observed by CD for each peptide can be explained as well, since the three-dimensional structures of sakacin P and sakP[N24C+44C] have shown that the same number of residues forms the α-helical part irrespective of whether the peptides were in TFE or in DPC.

Whereas the spectra of sakacin P in DPC were only amenable to interpretation once the sequential assignment of sakP[N24C+44C] was available, the spectra of sakacin P in 90% TFE displayed sharp line widths and were in general of relatively high quality. These spectra were especially useful for analyzing the N-terminal β-sheet structure, which was better defined in TFE than in DPC, as indicated by a lower rmsd over the backbone atoms of residues 6−16 (Table 1, Figure 3I). The C-terminal tail had, however, no clearly defined orientation in TFE.

Comparison with Leucocin A and Carnobacteriocin B2. Until now the only pediocin-like AMPs whose three-dimensional structures have been solved are leucocin A, a 37-residue peptide isolated from *Leuconostoc* (*14*), and carnobacteriocin B2, a 48-residue peptide isolated from *Carnobacterium piscicola* LV17B (*15*). The general structural arrangements of these four peptides, sakacin P, sakP-[N24C+44C], leucocin A, and carnobacteriocin B2, are similar. Their N-terminal regions show varying degrees of three-stranded antiparallel β-sheet structuring, with leucocin A and sakacin P (both in TFE) having perhaps the most well-defined β-sheet structure. SakP[N24C+44C] was not studied in TFE but will presumably have the same structure in the N-terminal region as sakacin P, since they have identical sequences in this region. The structure of carnobacteriocin B2 has only been reported in TFE, in which the N-terminal region showed very little well-defined structure (*15*). All four peptides have a central amphiphilic α-helix starting in residue 17/18 and ending in residue 31 in leucocin A, in residue 33 in sakP[N24C+44C] and sakacin P, and in residue 39 in carnobacteriocin B2. The C-terminal was unstructured in carnobacteriocin B2 and leucocin A in TFE, but it showed a tendency to fold back onto the helix in leucocin A in DPC (*14*, *15*), although in a different orientation with respect to the helix than what was observed for sakacin P and sakP-[N24C+44C]. Whether this difference is due to the lack of long-range NOEs in leucocin A or an intrinsic characteristic of its sequence is unclear.

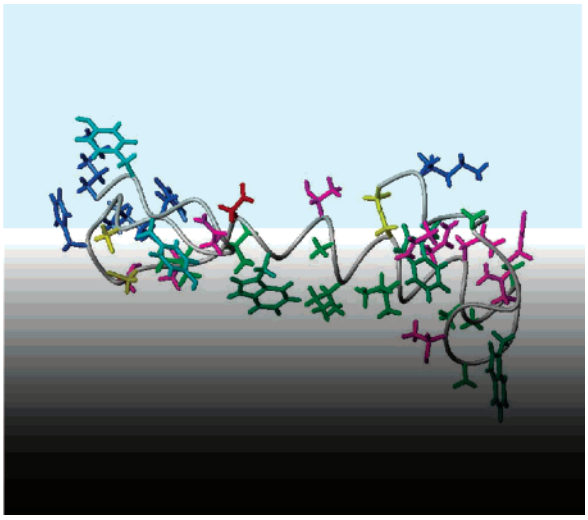

FIGURE 6: Model of the interaction of sakP[N24C+44C] with the membrane. The hydrophobic side chains insert into the membrane (gray), whereas the hydrophilic residues lie at the surface. The N-terminal part may move around the hinge at Asp17 (colored in red) and point to the aqueous outside (light blue). (Side chain coloring as in Figure 4).

Mode of Interaction with Membranes: The positively charged residues found on the same side of the N-terminal β-sheet appear to mediate the electrostatic interactions involved in the initial binding of pediocin-like AMPs to the negatively charged bacterial phospholipid-containing membrane and/or the acidic cell wall. Especially the cationic patch in the middle of the N-terminal region (Lys11 and His12 in sakacin P and sakP[N24C+44C]) appears to be of great importance for binding to target cells, as judged by mutational analysis (*11*) and peptide binding studies (*29*). It is thought that, after binding to the target cell membrane via the N-terminal region, the central amphiphilic α-helix and the C-terminal tail (i.e. the hairpin-like structure constituting the C-terminal half) may penetrate into the cell membrane and thereby permeabilize the membrane (6, *10*, *30*, *31*). The hinge between the β-sheetlike N-terminal region and the central helix might function to render enough structural flexibility to enable the hairpin-like C-terminal half to dip into the hydrophobic part of the membrane (Figure 6).

The notion that the hairpin-like C-terminal half penetrates into the membrane is supported by mutagenesis studies which show that hydrophilic residues are not readily introduced into this region without greatly reducing the antimicrobial activity (*6*, *13*, *32*, *33*). Trp33 may be replaced by a leucine residue but not by a hydrophilic or another aromatic residue, indicating that Trp33 inserts itself in the target membrane (*6*). Aromaticity at positions 18 and 41 in sakacin P was, however, much more important than hydrophobicity. This may indicate that Trp18 and 41 are positioned in the interface between the hydrophobic core of the membrane and the hydrophilic headgroups (*34*). Moreover, the interaction of Trp41 with Ile25 stabilizes the hairpin, and this explains why most pediocin-like AMPs that lack a tryptophan residue in the C-terminal tail have instead a C-terminal disulfide bridge similar to the one in sakP[N24C+44C] (*6*).

The mechanism by which the helix may contribute to membrane permeabilization has not been elucidated and is the subject of much debate. Amphiphilic helices may orient themselves parallel to the membrane surface or insert perpendicular into the membrane to form a pore. On the basis of our structural results, we are not able a priori to distinguish between the two hypothesis in an unambiguous way. Three arguments may, however, support a parallel attachment to the membrane: (a) The observed folding back of the C-terminus masks parts of the side chains of Ile25, Ala29, and Trp33. This reduces the hydrophobic surface of the amphiphilic helix and makes a perpendicular interaction with the membrane relatively unlikely. (b) If both Trp18 and 41 have to be in the interface, this can only be achieved by a parallel or oblique alignment with the membrane. (c) Since the α-helix is only comprised of 15 residues, a considerable rearrangement of the lipid bilayer would have to occur to orient sakacin P in such a way that Trp 18 at the beginning and Trp33 at the end of the helix are accommodated at opposite membrane interfaces.

Interestingly, by turning sakP[N24C+44C] in such a way that Trp18 and 41 are located at about the same level (for instance, the membrane−surface interface), while Trp33 is allowed to insert more deeply into the core of the membrane, the peptide obtains an oblique orientation that would not be very distinct from a parallel one (Figure 6). The turn starting from residue 34 positions Thr35 in our model toward the hydrophobic face of the peptide opposing a deeper penetration into the membrane. However, the conformation of this turn is defined by short-range distances only, and it is conceivable that it depends on the membrane-mimicking agent used. An oblique orientation of the central helical region has also been suggested on the basis of computer modeling (*30*) and mutagenesis analysis (*6*), and it might by itself interfere sufficiently with the close and correct packing of membrane hydrocarbons, thereby permeabilizing the membrane. The fact that the hairpin-like C-terminal half of pediocin-like AMPs both interacts with the hydrophobic core of the membrane and plays a major role in determining their target cell specificity supports the interesting notion that a cell's sensitivity to these AMPs may to a large extent be determined by the composition of the hydrophobic membrane core rather than by the functionality of a receptor or docking-site for the peptide on the surface of the cell.

CONCLUSION

We solved the structures of sakacin P and sakP-[N24C+44C] by NMR. The structural comparison shows that the two structures are alike, which implies that the C-terminus of sakacin P folds back onto the amphiphilic helix. The structural data may support a previously proposed model of an oblique orientation of pediocin-like bacteriocins with the target membrane. The structural models have been deposited with the protein data bank and can be retrieved under accession numbers 1OG7, 1OHN, and 1OHM for sakacin P in TFE, sakain P in DPC, and sakP[N24C+44C] in DPC, respectively.

ACKNOWLEDGMENT

H.H.H. thanks Dr. Michael Nilges of the Institut Pasteur, Paris, for initial support and Dr. Maria Macias, EMBL, for recording some of the NMR spectra of sakacin P in TFE. C.M.-G. is supported by a grant from the DFG (Mu-1606).

SUPPORTING INFORMATION AVAILABLE

Three tables of ^{1}H chemical shifts of sakP[N24C+44C] in DPC micelles and of sakacin P in DPC micelles and 90% TFE. This material is available free of charge via the Internet at http://pubs.acs.org.

REFERENCES

1. Nissen-Meyer, J., and Nes, I. F. (1997) Ribosomally synthesized antimicrobial peptides: Their function, structure, biogenesis, and mechanism of action, *Arch. Microbiol. 167*, 67−77.
2. Nes, I. F., Diep, D. B., Håvarstein, L. S., Brurberg, M. B., Eijsink, V., and Holo, H. (1996) Biosynthesis of bacteriocins in lactic acid bacteria, *Antonie van Leeuwenhoek 70*, 113−128.
3. Nes, I. F., Holo, H., Fimland, G., Hauge, H. H., and Nissen-Meyer, J. (2002) Unmodified peptide-bacteriocins (class II) produced by lactic acid bacteria, in *Peptide antibiotics, Discovery, modes of action and application* (Dutton, Haxell, McArthur, and Wax, Eds.), Marcel Decker, Inc., New York.
4. Ennahar, S., Sashihara, T., Sonomoto, K., and Ishizaki, A. (2000) Class IIa bacteriocins: Biosynthesis, structure and activity, *FEMS Microbiol. Rev. 24*, 85−106.
5. Nissen-Meyer, J., Hauge, H. H., Fimland, G., Eijsink, V. G. H., and Nes, I. F. (1997) Ribosomally synthesized antimicrobial peptides produced by lactic acid bacteria: Their function, structure, biogenesis, and their mechanism of action, *Recent. Res. Dev. Microbiol. 1*, 141−154.
6. Fimland, G., Eijsink, V. G. H., and Nissen-Meyer, J. (2002) Mutational analysis of the role of tryptophan residues in an antimicrobial peptide, *Biochemistry 41*, 9508−9515.
7. Moll, G. N., Konings, W. N., and Driessen, A. J. M. (1999) Bacteriocins: Mechanism of membrane insertion and pore formation, *Antonie van Leeuwenhoek 76*, 185−98.
8. Chikindas, M. L., Garcia-Garcera, M. J., Driessen, A. J. M., Ledeboer, A. M., Nissen-Meyer, J., Nes, I. F., Abee, T., Konings, W. N., and Venema, G. (1993) Pediocin PA-1, a bacteriocin from *Pediococcus acidilactici* PAC1.0, forms hydrophillic pores in the cytoplasmic membrane of target cells, *Appl. Environ. Microbiol. 59*, 3577−3584.
9. Eijsink, V. G. H., Skeie, M., Middelhoven, H., Brurberg, M. B., and Nes, I. F. (1998) Comparative studies of pediocin-like bacteriocins, *Appl. Environ. Microbiol. 64*, 3275−3281.
10. Fimland, G., Blingsmo, O. R., Sletten, K., Jung, G., Nes, I. F., and Nissen-Meyer, J. (1996) New biologically active hybrid bacteriocins constructed by combining regions from various pediocin-like bacteriocins: the C-terminal region is important for determining specificity, *Appl. Environ. Microbiol. 62*, 3313−3318.
11. Kazazic, M., Nissen-Meyer, J., and Fimland, G. (2002) Mutational analysis of the role of charged residues in target-cell-binding, potency and specificity of the pediocin-like bacteriocin sakacin P, *Microbiology 148*, 2019−2026.
12. Fimland, G., Johnsen, L., Axelsson, L., Brurberg, M. B., Nes, I. F., Eijsink, V. G. H., and Nissen-Meyer, J. (2000) A C-terminal disulfide bridge in pediocin-like bacteriocins renders bacteriocin activity less temperature dependent and is a major determinant of the antimicrobial spectrum, *J. Bacteriol. 182*, 2643−2648.
13. Johnsen, L., Fimland, G., Eijsink, V., and Nissen-Meyer, J. (2000) Engineering increased stability in the antimicrobial peptide pediocin PA-1, *Appl. Environ. Microbiol. 66*, 4798−4802.
14. Fregeau Gallagher, N. L., Sailer, M., Niemczura, W. P., Nakashima, T. T., Stiles, M. E., and Vederas, J. C. (1997) Three-dimensional structure of leucocin A in trifluoroethanol and dodecylphosphocholine micelles: Spatial location of residues critical for biological activity in type IIa bacteriocins from lactic acid bacteria, *Biochemistry 36*, 15062−15072.
15. Wang, Y., Henz, M. E., Fregeau Gallagher, N. L., Chai, S., Gibbs, A. C., Liang, Z. Y., Stiles, M. E., Wishart, D. S., and Vederas, J. C. (1999) Solution structure of carnobacteriocin B2 and implications for structure−activity relationships among type IIa bacteriocins from lactic acid bacteria, *Biochemistry 38*, 15438−15447.
16. Hühne, K., Axelsson, L., Holck, A., and Kröckel, L. (2001) Analysis of the sakacin P gene cluster from *Lactobacillus sake*

Lb674 and its expression in sakacin-negative *Lb. sake* strains, *Microbiology 142*, 1437−1448.
17. van de Guchte, M., van der Vossen, J. M. B. M., Kok, J., and Venema, G. (1989) Construction of a lactococcal expression vector: expression of hen egg white lysozyme in *Lactococcus lactis* subsp. *Lactis*, *Appl. Environ. Microbiol. 55*, 224−228.
18. Uteng, M., Hauge, H. H., Brondz, I., Nissen-Meyer, J., and Fimland, G. (2002) Rapid two-step procedure for large-scale purification of pediocin-like bacteriocins and other cationic antimicrobial peptides from complex culture medium, *Appl. Environ. Appl. Environ. Microbiol. 68*, 952−956.
19. Chen, Y. H., Yang, J. T., and Chau, K. H. (1974). Determination of the helix and beta forms of proteins in aqueous solution by circular dichroism, *Biochemistry 13*, 3350−3359.
20. Cavanagh, J., and Rance, M. (1992) Suppression of cross-relaxation effects in TOCSY spectra via a modified DIPSI-2 mixing sequence, *J. Magn. Reson. 96*, 670−665.
21. Piotto, M., Daudek, V., and Sklenar, V. (1992) Gradient tailored excitation for single-quantum NMR spectroscopy of aqueous solutions, *J. Biomol. NMR 2*, 661−665.
22. Bartels, C., Xia, T.-H., Billeter, M., Güntert, P., and Wüthrich, K. (1995). The program XEASY for computer-supported NMR spectral analysis of bilogical macromolecules, *J. Biomol. NMR 5*, 1−10.
23. Brünger, A. T., Adams, P. D., Clore, G. M., Delano, W. L., Gros, P., Grosse-Kunstleve, R. W., Jiang, J. S., Kuszewski, J., Nilges, M., Pannu, N. S., Read, R. J., Rice, L. M., Simonson, T., and Warren, G. L. (1998) Crystallography and NMR system: A new software suit for macromolecular structure determination, *Acta Crystallogr., Sect. D: Biol. Crystallogr. 54*, 905−92.
24. Linge, J. P., Habeck, M., Rieping, W., and Nilges, M. (2003) ARIA: automated NOE assignment and NMR structure calculation, *Bioinformatics 19*, 315−316.
25. Linge, J. P., and Nilges, M. (1999) Influence of nonbonded parameters on the quality of NMR structures: a new force field for NMR structure calculation, *J. Biomol. NMR 13*, 51−59.
26. Case, D. A., Pearlman, D. A., Caldwell, J. C., III, Cheatham, T. E., Ross, W. S., Simmerling, C. L., Darden, T. A., Merz, T. M., Stanton, R. V., Cheng, A. L., Vincent, J. J., Crowley, M., Tsui, V., Radmer, R. J., Duan, Y., Pitera, J., Massova, I., Seibel, G. L., Singh, U. C., Weiner, P. K., and Kollman, P. A. (1999) *AMBER 6*, University of California, San Francisco.
27. Tsui, V., and Case, D. A (2000). *J. Am. Chem. Soc. 122*, 2489−2498.
28. Koradi, R., Billeter, M., and Wüthrich, K. (1996) MOLMOL: A program for display and analysis of macromolecular structure, *J. Mol. Graphics 14*, 51−55.
29. Chen, Y., Ludescher, R. D., and Montville, T. J. (1997) Electrostatic interactions, but not the YGNGV consensus motif, govern the binding of pediocin PA-1 and its fragments to phospholipid vesicles, *Appl. Environ. Microbiol. 63*, 4770−4777.
30. Bennik, M. H. J., Vanloo, B., Brasseur, R., Gorris, L. G. M., and Smid, E. J. (1998) A novel bacteriocin with a YGNGV motif from vegetable-associated *Enterococcus mundtii*: full characterization and interaction with target organisms, *Biochim. Biophys. Acta 1373*, 47−58.
31. Miller, K. W., Schamber, R., Chen, Y., and Ray, B. (1998) Production of active chimeric pediocin AcH in *Escherichia coli* in the absence of processing and secretion genes from the *pediococcus pap* operon, *Appl. Environ. Microbiol. 64*, 14−20.
32. Miller, K. W., Schamber, R., Osmanagaoglu, O., and Ray, B. (1998) Isolation and characterization of pediocin AcH chimeric protein mutants with altered bactericidal activity, *Appl. Environ. Microbiol. 64*, 1997−2005.
33. Quadri, L. E. N., Yan, L. Z., Stiles, M. E., and Vederas, J. C. (1997) Effect of amino acid substitutions on the activity of carnobacteriocin B2, *J. Biol. Chem. 272*, 3384−3388.
34. Kilian, J. A., and von Heijne, G. (2000) How proteins adapt to a membrane-water interface, *Trends Biochem. Sci. 25*, 429−434.

BI034572I